To cite this article: ZHANG Q, ZHU Y P, MENG X F, et al. Finite time trajectory tracking of underactuated ship based on adaptive neural network[J/OL]. Chinese Journal of Ship Research, 2022, 17(4). http://www. ship-research. com/en/article/doi/10.19693/j.issn.1673-3185.02564.

DOI: 10.19693/j.issn.1673-3185. 02564

Finite time trajectory tracking of underactuated ship based on adaptive neural network

ZHANG Qiang, ZHU Yaping, MENG Xiangfei, ZHANG Shuhao, HU Yancai*

School of Navigation and Shipping, Shandong Jiaotong University, Weihai 264200, China

Abstract: [**Objective**] Aiming at the problems of dynamic uncertainty and unknown disturbance in the trajectory tracking control of underactuated surface ships, a finite time trajectory tracking control scheme based on an adaptive neural network is designed. [**Method**] The underactuated variation is carried out by using the method of kinematic virtual control law transformation and bounded constraints. Under the framework of Backstepping, neural networks are used to reconstruct unknown dynamics, and an adaptive law is designed to approach the upper bound of unknown disturbances. The Lyapunov direct method provides a rigorous theoretical analysis that proves that all the signals of the closed-loop system are bounded, and the tracking error converges to a bounded interval. [**Results**] The simulation results show that this control scheme can make an underactuated ship track the desired trajectory in a limited time, and the convergence speed of the system error is faster than that of the traditional control scheme. The upper and lower bounds of the error are also smaller. It also shows good robustness in the face of unknown time-varying interference from the outside world. [**Conclusion**] The results of this study can provide valuable references for the tracking and control of ship trajectories and are of great practical engineering significance.

Key words: trajectory tracking; adaptive neural network; finite time; unknown disturbance; underactuated surface ship

CLC number: U675.91

0 Introduction

There is an increasing demand for the exploitation, transportation, and exploration of marine resources with the development of science and technology. As an economical and effective tool, surface ships play a crucial role in marine engineering. As a typical control task in ship motion control, trajectory tracking control enables surface ships to track the required reference trajectories. As surface ships are widely used, trajectory tracking control has also gained wide attention from scholars both in China and abroad. As surface ships will meet disturbances from various internal and external uncertainties during navigation, it is quite necessary to take into account the influences of these complex factors

Received: 2020 – 10 – 24 **Accepted**: 2021 – 12 – 24

Supported by: National Natural Science Foundation of China (51911540478); Key Research & Development Program of Shandong Province (2019JZZY020712); Postgraduate Education & Teaching Reform Research Project of Shandong Province (SDYJG19217); Doctoral Research and Entrepreneurship Fund of Shandong Jiaotong University; and Program of Climbing Research and Innovation Team of Shandong Jiaotong University (SDJTUC1802)

Authors: ZHANG Qiang, male, born in 1982, Ph.D., professor. Research interest: motion and control of ships and robots. E-mail: zq20060054@163.com

ZHU Yaping, female, born in 1996, master degree. Research interest: ship motion and control. E-mail: yapingzhu514@163.com

MENG Xiangfei, male, born in 1991, master degree. Research interest: ship motion and control. E-mail: brucem2021@126.com

ZHANG Shuhao, male, born in 1983, lecturer. Research interest: ship motion control and intelligent navigation technology. E-mail: zsh5225@163.com

HU Yancai, male, born in 1987, Ph.D., lecturer. Research interest: ship motion and control. E-mail: yancaihu@126.com

***Corresponding author**: ZHANG Shuhao

in the design of the trajectory tracking control. As a result, various advanced control methods have been applied to the design of trajectory tracking control schemes.

The field of trajectory tracking of fully actuated ships sees the application of the trajectory linearization control method [1], the control method for dynamic surface adaptive neural network control of ship trajectory tracking based on nonlinear gain recursion sliding mode [2], and the control method for the minimum parameter adaptive recursion sliding mode based on Lyapunov function of time-varying asymmetric obstacles [3], and these methods aim to solve the problem of trajectory tracking control of surface ships. They have not only served as a solution to the problem concerning the trajectory tracking of fully actuated ships with uncertain conditions and unknown parameters but also enhanced the tracking accuracy. As the sea surface is dominated by underactuated ships, studies in this regard are of great significance to reducing costs and improving shipping safety. For the problem concerning the trajectory tracking of underactuated surface ships, Meng et al. [4] solved the robustness problem caused by the uncertainty of model parameters and unknown disturbances by introducing the control law of sliding plane design. Shen et al. [5] proposed the dynamic surface adaptive output feedback control and ensured the uniformly ultimate boundedness (UUB) of the ship trajectory tracking error by introducing an observer. The model predictive control (MPC) proposed by Liu et al. [6] achieved the approximate linearization of the model. However, the method reported more significant tracking errors when the external disturbance coefficient became larger. References [7-8] realized robust adaptive control by using an observer and proportional integral, respectively, and Reference [8] also further reduced the vibration caused by sliding mode control. Dai et al. [9] estimated the unknown disturbances by introducing a disturbance observer, and Haseltable et al. [10] further improved the accuracy of trajectory tracking by introducing a neural network to approximate the nonlinear function.

The above references, however, can only get an asymptotically stable result when the system time tends to infinity, without taking into account whether the ship can achieve finite-time tracking control under the influence of various uncertainties. Wang et al. [11] introduced a decentralized controller based on terminal sliding mode control and proposed a terminal sliding mode control method, which enabled underactuated surface ships to track and maintain the desired trajectory fast within a finite time. Ning et al. [12] first encapsulated the unknown parameter dynamics and uncertainties into nonlinear functions and then identified the nonlinear functions online via an adaptive fuzzy approach, and thus they obtained a new direct adaptive fuzzy tracking control method, which enabled the tracking by ships within a finite time. Sun et al. [13] proposed a robust fuzzy adaptive definite performance finite-time control method that was event-triggered. Zhao et al. [14] designed the adaptive finite-time control laws with and without boundary layers for the rigid spacecraft with unknown upper-bound disturbances, achieved trajectory tracking within a finite time, and eliminated the buffeting.

Based on the above analyses, this paper intends to design a finite-time trajectory tracking control scheme based on an adaptive neural network under the influence of dynamic uncertainties and unknown time-varying disturbances. First, we use the radial basis function (RBF) neural network to reconstruct the dynamic uncertainties of the ship and design an adaptive law to approximate the upper bound of the unknown disturbances. Due to the high fitting relationship between the RBF neural network and the nonlinear function, it is necessary to improve the approximation accuracy and introduce the finite-time control theory into the control scheme design to ensure that the system tracking error can converge to a relatively small area within a finite time, and thus the convergence speed of the system error can be improved. Finally, we carry out the simulation comparison tests to verify the tracking effect of the control scheme.

1 Mathematical model of the ship and problem description

We here consider the following mathematical model of underactuated surface ships [15]:

$$\begin{cases} \dot{x} = u\cos(\psi) - v\sin(\psi) \\ \dot{y} = u\sin(\psi) + v\cos(\psi) \\ \dot{\psi} = r \end{cases} \tag{1}$$

$$\begin{cases} \dot{u} = f_u(u,v,r) + \dfrac{1}{m_u}[\tau_u + d_u] \\ \dot{v} = f_v(u,v,r) + \dfrac{1}{m_v} d_v \\ \dot{r} = f_r(u,v,r) + \dfrac{1}{m_r}[\tau_r + d_r] \end{cases} \tag{2}$$

and

$$\begin{cases} f_u(\boldsymbol{u},\boldsymbol{v},\boldsymbol{r}) = \dfrac{1}{m_u}(m_v\boldsymbol{v}\boldsymbol{r} - \boldsymbol{Y}_{\dot{r}}\boldsymbol{r}^2 + \boldsymbol{X}_u\boldsymbol{u} + \boldsymbol{X}_{u|u|}|\boldsymbol{u}|\boldsymbol{u}) \\ f_v(\boldsymbol{u},\boldsymbol{v},\boldsymbol{r}) = \dfrac{1}{m_v}(\boldsymbol{Y}_v\boldsymbol{v} + \boldsymbol{Y}_{|v|v}|\boldsymbol{v}|\boldsymbol{v} + \boldsymbol{Y}_{|r|v}|\boldsymbol{r}|\boldsymbol{v} + \\ \qquad \boldsymbol{Y}_r\boldsymbol{r} - m_u\boldsymbol{u}\boldsymbol{r} + \boldsymbol{Y}_{|v|r}|\boldsymbol{v}|\boldsymbol{r} + \boldsymbol{Y}_{|r|r}|\boldsymbol{r}|\boldsymbol{r} \\ f_r(\boldsymbol{u},\boldsymbol{v},\boldsymbol{r}) = \dfrac{1}{m_r}[(m_u - m_v)\boldsymbol{u}\boldsymbol{v} + \boldsymbol{Y}_{\dot{r}}\boldsymbol{u}\boldsymbol{r} + \boldsymbol{N}_v\boldsymbol{v} + \\ \qquad \boldsymbol{N}_r + \boldsymbol{N}_{|r|v}|\boldsymbol{r}|\boldsymbol{v} + \boldsymbol{N}_{|v|v}|\boldsymbol{v}|\boldsymbol{v} + \boldsymbol{N}_{|r|r}|\boldsymbol{r}|\boldsymbol{r}] \end{cases} \tag{3}$$

where $\boldsymbol{x}$, $\boldsymbol{y}$, and $\boldsymbol{\psi}$ serve as the actual tracking trajectory of the surface ship, and they represent the lateral displacement, longitudinal displacement, and course angle, respectively; $\boldsymbol{u}$, $\boldsymbol{v}$, and $\boldsymbol{r}$ refer to the actual tracking velocity, and they represent the forward speed, sway speed, and heading rate, respectively; $\boldsymbol{\tau}_u$ represents the surge control force of the ship; $\boldsymbol{\tau}_r$ represents the yaw control moment; $\boldsymbol{m}_u$, $\boldsymbol{m}_v$ and $\boldsymbol{m}_r$ represent the added mass; $\boldsymbol{d}_u$ and $\boldsymbol{d}_r$ are the disturbances; f_u ($\boldsymbol{u}$, $\boldsymbol{v}$, $\boldsymbol{r}$), f_v ($\boldsymbol{u}$, $\boldsymbol{v}$, $\boldsymbol{r}$), and f_r ($\boldsymbol{u}$, $\boldsymbol{v}$, $\boldsymbol{r}$) are the unknown dynamics; $\boldsymbol{X}_u$, $\boldsymbol{Y}_v$, $\boldsymbol{Y}_r$, $\boldsymbol{N}_v$, and $\boldsymbol{N}_r$ stand for the linear damping of the surface ship in the forward, sway, and yaw dimensions, respectively; $\boldsymbol{X}_{u|u|}|\boldsymbol{u}|\boldsymbol{u}$, $\boldsymbol{Y}_{|v|v}|\boldsymbol{v}|\boldsymbol{v}$, $\boldsymbol{Y}_{|r|v}|\boldsymbol{r}|\boldsymbol{v}$, $\boldsymbol{Y}_{|v|r}|\boldsymbol{v}|\boldsymbol{r}$, $\boldsymbol{N}_{|r|r}|\boldsymbol{r}|\boldsymbol{r}$, and $\boldsymbol{N}_{|r|v}|\boldsymbol{r}|\boldsymbol{v}$ stand for the nonlinear damping of the surface ship in the forward, sway, and yaw dimensions, respectively.

In order to achieve the design of the controller, we give the following assumptions, definitions, and lemmas.

Definition: The nonlinear control system is described as follows:

$$\dot{\boldsymbol{x}} = f(\boldsymbol{x}),\ \boldsymbol{x}(0) = x_0,\ \boldsymbol{x} \in \Omega_0 \subset \mathbf{R}^n \tag{4}$$

where $\boldsymbol{x} \in \mathbf{R}^n$ represents the state variable of the system; Ω_0 is a sphere containing the origin; $f(\boldsymbol{x})$ is a continuous function. For any initial condition x_0, if there is a constant $\zeta > 0$ and a time regulation function $0 < T(0) < \infty$ that makes $\|x(t)\| \leqslant \zeta$ and $t \geqslant T(x_0)$, then the system can be considered to be stable in semi-global real finite time [16]. Specifically, t represents the time variable, and T is the time under the initial conditions.

Lemma 1: In terms of a system $\boldsymbol{x} = f(\boldsymbol{x})$, $f(0) = 0$, $\boldsymbol{x} \in \mathbf{R}^n$, where $f(\boldsymbol{x})$ represents a continuous function, if there is a continuous Lyapunov function V: $D \to \mathbf{R}$ that can satisfy the following conditions: V represents a positive definite function, and there is a real number $\rho_1 > 0$, $\rho_2 > 0$, $\eta \in (0, 1)$, and an open-loop neighborhood near the origin satisfies $\dot{V}(\boldsymbol{x}) + \rho_1 V(\boldsymbol{x}) + \rho_2 V^{\eta}(\boldsymbol{x}) \leqslant 0$, then the system is stable in finite time, and the stability time T_r is [17]

$$T_r = \frac{1}{\rho_1(1-\eta)}\ln\frac{\rho_1 V^{1-\eta}(\boldsymbol{x}) + \rho_2}{\rho_2} \tag{5}$$

Lemma 2: For any given continuous smooth function $\boldsymbol{h}(\boldsymbol{x})$ defined on the compact set $\Omega \subset \mathbf{R}^n$ [18-19],

$$h(\boldsymbol{x}) = \boldsymbol{W}^{*\mathrm{T}} s(\boldsymbol{x}) + \boldsymbol{\varepsilon},\ \forall \boldsymbol{x} \in \Omega \tag{6}$$

where ε represents the approximation error, and for all $\boldsymbol{x} \in \Omega$, there is a vector $\boldsymbol{\varepsilon}^* > 0$, which meets $|\boldsymbol{\varepsilon}| \leqslant \boldsymbol{\varepsilon}^*$; $\boldsymbol{W}^*$ represents the weight vector under ideal conditions; $s(\boldsymbol{x})$ is the central function. In general, the ideal neural network weight is an unknown vector, which needs to be estimated. It can be interpreted as $\boldsymbol{W}$ that can minimize $|\boldsymbol{\varepsilon}|$ on $\boldsymbol{x} \in \Omega \subset \mathbf{R}^n$, i.e.

$$\boldsymbol{W}^* = \underset{\boldsymbol{W} \in \mathbf{R}^L}{\operatorname{argmin}}\left\{\sup_{\boldsymbol{x} \in \mathbf{R}}|h(\boldsymbol{x}) - \boldsymbol{W}^{\mathrm{T}} s(\boldsymbol{x})|\right\} \tag{7}$$

Lemma 3: For any $a > 0$ (a is a constant) and $\boldsymbol{x} \in \mathbf{R}$, the following relationship is satisfied [20]:

$$0 < |\boldsymbol{x}| - \boldsymbol{x}\tanh\left(\frac{\boldsymbol{x}}{a}\right) \leqslant 0.278\,5a \tag{8}$$

2 Design of the controller

The flow of trajectory tracking control is shown in Fig. 1. In order to solve the problem of underactuation, we adopt the method in Reference[21]. First, we define the tracking error of underactuated surface ships as follows:

$$\begin{cases} \boldsymbol{x}_e = \boldsymbol{x} - \boldsymbol{x}_1 \\ \boldsymbol{y}_e = \boldsymbol{y} - \boldsymbol{y}_1 \\ \boldsymbol{\psi}_e = \boldsymbol{\psi} - \boldsymbol{\psi}_1 \end{cases} \tag{9}$$

$$\begin{cases} \boldsymbol{u}_e = \boldsymbol{u} - \boldsymbol{u}_1 \\ \boldsymbol{r}_e = \boldsymbol{r} - \boldsymbol{r}_1 \end{cases} \tag{10}$$

where $\boldsymbol{x}_1$, $\boldsymbol{y}_1$, and $\boldsymbol{\psi}_1$ represent the expected lateral displacement, expected longitudinal displacement, and expected course angle in the tracking process; $\boldsymbol{u}_1$ and $\boldsymbol{r}_1$ represent the expected forward speed and the expected heading rate during the tracking, respectively.

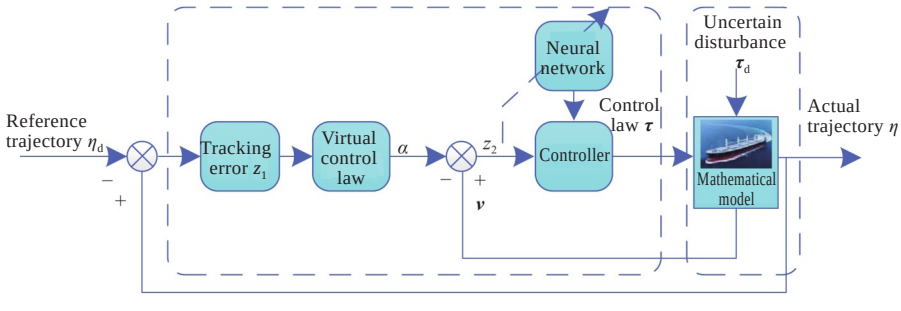

Fig. 1 Trajectory tracking control flow chart

We let

$$z_{\mathrm{e}}=\begin{bmatrix} x_{\mathrm{e}} \\ y_{\mathrm{e}} \end{bmatrix}=\begin{bmatrix} x-x_1 \\ y-y_1 \end{bmatrix} \tag{11}$$

By deriving Eq. (11), we have

$$\dot{z}_{\mathrm{e}}=\boldsymbol{u}\boldsymbol{g}_u(\varphi)+v\boldsymbol{g}_v(\varphi)-\begin{pmatrix} \dot{x}_1 \\ \dot{y}_1 \end{pmatrix} \tag{12}$$

where $\boldsymbol{g}_u(\varphi)=\begin{bmatrix} \cos(\varphi) \\ \sin(\varphi) \end{bmatrix}$; $\boldsymbol{g}_v(\varphi)=\begin{bmatrix} -\sin(\varphi) \\ \cos(\varphi) \end{bmatrix}$.

To stabilize the errors z_{e} and $\boldsymbol{\psi}_{\mathrm{e}}$, we construct the Lyapunov function $V_1=\frac{1}{2}{z_{\mathrm{e}}}^2+\frac{1}{2}{\boldsymbol{\psi}_{\mathrm{e}}}^2$, with the virtual variables α and α_r designed, as shown in Eq. (13).

$$\begin{cases} \alpha=-k_{11}z_{\mathrm{e}}-\dfrac{k_{12}z_{\mathrm{e}}}{\sqrt{\|z_{\mathrm{e}}\|^2+\delta^2}}-v\boldsymbol{g}_v(\boldsymbol{\psi})+\begin{pmatrix} \dot{x}_1 \\ \dot{y}_1 \end{pmatrix} \\ \alpha_r=-k_{31}\boldsymbol{\psi}_{\mathrm{e}}-\dfrac{k_{32}\boldsymbol{\psi}_{\mathrm{e}}}{\sqrt{\|\boldsymbol{\psi}_{\mathrm{e}}\|^2+\delta^2}}+\dot{\boldsymbol{\psi}}_1 \end{cases} \tag{13}$$

where k_{11}, k_{12}, k_{31}, k_{32}, and δ are adjustable parameters.

We design the desired forward speed, heading rate, and course angle according to Eq. (13):

$$\begin{cases} \boldsymbol{u}_1=\|\alpha\| \\ \boldsymbol{r}_1=-k_{31}\boldsymbol{\psi}_{\mathrm{e}}-\dfrac{k_{32}\boldsymbol{\psi}_{\mathrm{e}}}{\sqrt{\|\boldsymbol{\psi}_{\mathrm{e}}\|^2+\delta^2}}+\dot{\boldsymbol{\psi}}_1 \\ \boldsymbol{\psi}_1=\arctan(\alpha_y,\alpha_x) \end{cases} \tag{14}$$

where $\boldsymbol{\psi}_1$ is obtained through the inverse solution of $\boldsymbol{u}_1=\|\alpha\|$; α_x and α_y are the components of α in the x and y directions.

By deriving Eq. (10), we can obtain

$$\begin{cases} \dot{\boldsymbol{u}}_{\mathrm{e}}=f_u(\boldsymbol{u},\boldsymbol{v},\boldsymbol{r})+\dfrac{1}{m_u}(\boldsymbol{\tau}_u+\boldsymbol{d}_u)-\dot{\boldsymbol{u}}_1= \\ \qquad f_u(\boldsymbol{u},\boldsymbol{v},\boldsymbol{r})+\dfrac{\boldsymbol{\tau}_u}{m_u}-\dot{\boldsymbol{u}}_1+\boldsymbol{\tau}_{d,u} \\ \dot{\boldsymbol{r}}_{\mathrm{e}}=f_r(\boldsymbol{u},\boldsymbol{v},\boldsymbol{r})+\dfrac{1}{m_r}(\boldsymbol{\tau}_r+\boldsymbol{d}_r)-\dot{\boldsymbol{r}}_1= \\ \qquad f_r(\boldsymbol{u},\boldsymbol{v},\boldsymbol{r})+\dfrac{\boldsymbol{\tau}_r}{m_r}-\dot{\boldsymbol{r}}_1+\boldsymbol{\tau}_{d,r} \end{cases} \tag{15}$$

For unknown dynamics $f_u(\boldsymbol{u}, \boldsymbol{v}, \boldsymbol{r})$ and $f_r(\boldsymbol{u}, \boldsymbol{v}, \boldsymbol{r})$, they are reconstructed by the RBF neural network, i.e.,

$$\begin{cases} f_u(\boldsymbol{u},\boldsymbol{v},\boldsymbol{r})={\boldsymbol{W}_u}^{\mathrm{T}}\sigma(\eta)+\boldsymbol{\varepsilon}_u \\ f_r(\boldsymbol{u},\boldsymbol{v},\boldsymbol{r})={\boldsymbol{W}_r}^{\mathrm{T}}\sigma(\eta)+\boldsymbol{\varepsilon}_r \end{cases} \tag{16}$$

where the network input signal $\eta=(\boldsymbol{x}, \boldsymbol{y}, \boldsymbol{\psi}, \boldsymbol{u}, \boldsymbol{v}, \boldsymbol{r})^{\mathrm{T}}$; $\sigma(\eta)$ represents the central function in the adaptive law of the weight of the neural network; the matrices of the weight of the neural network are $\boldsymbol{W}_u=(w_{u1}, w_{u2}, \cdots, w_{uh})^{\mathrm{T}}$ and $\boldsymbol{W}_r=(w_{r1}, w_{r2}, \cdots, w_{rh})^{\mathrm{T}}$, respectively; $\boldsymbol{\varepsilon}_u$ and $\boldsymbol{\varepsilon}_r$ represent the approximation errors of the neural network.

In order to stabilize $\boldsymbol{u}_e$ and $\boldsymbol{r}_e$, we design a control law, as shown in Eq. (17):

$$\begin{cases} \boldsymbol{\tau}_u=m_u\left[-k_{21}\boldsymbol{u}_{\mathrm{e}}-\dfrac{k_{22}\boldsymbol{u}_{\mathrm{e}}}{\sqrt{\|\boldsymbol{u}_{\mathrm{e}}\|^2+\varsigma^2}}-\right. \\ \qquad \left.\hat{\boldsymbol{W}}_u^{\mathrm{T}}\sigma(\eta)+\dot{\boldsymbol{u}}_1-\mathrm{Tanh}\left(\dfrac{\boldsymbol{u}_{\mathrm{e}}}{\varpi_u}\right)\hat{\bar{\boldsymbol{\delta}}}_u\right] \\ \boldsymbol{\tau}_r=m_r\left[-k_{41}\boldsymbol{r}_{\mathrm{e}}-\dfrac{k_{42}\boldsymbol{r}_{\mathrm{e}}}{\sqrt{\|\boldsymbol{r}_{\mathrm{e}}\|^2+\varsigma^2}}-\right. \\ \qquad \left.\hat{\boldsymbol{W}}_r^{\mathrm{T}}\sigma(\eta)-\boldsymbol{\psi}_{\mathrm{e}}+\dot{\boldsymbol{u}}_1-\mathrm{Tanh}\left(\dfrac{\boldsymbol{r}_{\mathrm{e}}}{\varpi_r}\right)\hat{\bar{\boldsymbol{\delta}}}_r\right] \end{cases} \tag{17}$$

where $\boldsymbol{\delta}_u=\boldsymbol{\varepsilon}_u+\boldsymbol{\tau}_{d,u}$; $\boldsymbol{\delta}_r=\boldsymbol{\varepsilon}_r+\boldsymbol{\tau}_{d,r}$; $\hat{\bar{\boldsymbol{\delta}}}_u$ and $\hat{\bar{\boldsymbol{\delta}}}_r$ represent the upper bound estimation of disturbances; $\hat{\boldsymbol{W}}_u$ and $\hat{\boldsymbol{W}}_r$ are the weight estimation value of the neural network; ς, k_{21}, k_{22}, k_{41}, and k_{42} are the adjustable parameters of the controller.

We design the following adaptive law:

$$\begin{cases} \dot{\hat{\boldsymbol{W}}}_u=\gamma_{w_u}[\boldsymbol{u}_{\mathrm{e}}\sigma(\eta)-\lambda_{w_u}\|\boldsymbol{u}_{\mathrm{e}}\|\hat{\boldsymbol{W}}_u] \\ \dot{\hat{\boldsymbol{W}}}_r=\gamma_{w_r}[\boldsymbol{r}_{\mathrm{e}}\sigma(\eta)-\lambda_{w_r}\|\boldsymbol{r}_{\mathrm{e}}\|\hat{\boldsymbol{W}}_r] \end{cases} \tag{18}$$

$$\begin{cases} \dot{\hat{\bar{\boldsymbol{\delta}}}}_u=\gamma_{d_u}\left(\mathrm{Tanh}\left(\dfrac{\boldsymbol{u}_{\mathrm{e}}}{\varpi_u}\right)\boldsymbol{u}_{\mathrm{e}}-\lambda_{d_u}\hat{\bar{\boldsymbol{\delta}}}_u\right) \\ \dot{\hat{\bar{\boldsymbol{\delta}}}}_r=\gamma_{d_r}\left(\mathrm{Tanh}\left(\dfrac{\boldsymbol{r}_{\mathrm{e}}}{\varpi_r}\right)\boldsymbol{r}_{\mathrm{e}}-\lambda_{d_r}\hat{\bar{\boldsymbol{\delta}}}_u\right) \end{cases} \tag{19}$$

where $\hat{\boldsymbol{W}}_u$ represents the estimated value of $\boldsymbol{W}_u$, and $\hat{\boldsymbol{W}}_u$ is bounded. In addition, there is a compact set $\Omega_{W_u}=\left\{\hat{\boldsymbol{W}}_u \middle| \|\hat{\boldsymbol{W}}_u\|\leqslant\overline{\boldsymbol{W}}_u/\varepsilon\right\}$, where $\overline{\boldsymbol{W}}_u>0$, and it represents the upper bound of $\|\sigma(\eta)\|$. Since $\hat{\boldsymbol{W}}_u$ and $\boldsymbol{W}_u$ are bounded, the weight estimation error of the neural network $\left(\tilde{\boldsymbol{W}}_u=\boldsymbol{W}_u-\hat{\boldsymbol{W}}_u\right)$ is also bounded in the system. The design parameters k_{21}, k_{22}, k_{41}, k_{42}, γ_{w_u},γ_{w_r},γ_{d_u} and γ_{d_r} are larger than zero.

3 Stability analysis

In order to verify the stability of the underactuated ship controller, the Lyapunov function presented in Eq. (20) is designed

$$V=\frac{1}{2}{z_{\mathrm{e}}}^{\mathrm{T}}z_{\mathrm{e}}+\frac{1}{2}{\boldsymbol{\psi}_{\mathrm{e}}}^2+\frac{1}{2}{\boldsymbol{u}_{\mathrm{e}}}^2+\frac{1}{2}{\boldsymbol{r}_{\mathrm{e}}}^2+\frac{1}{2\gamma_{d_u}}{\tilde{\bar{\boldsymbol{\delta}}}_u}^2+\frac{1}{2\gamma_{d_r}}{\tilde{\bar{\boldsymbol{\delta}}}_r}^2 \tag{20}$$

where $\tilde{\bar{\boldsymbol{\delta}}}_u=\bar{\boldsymbol{\delta}}_u-\hat{\bar{\boldsymbol{\delta}}}_u$, $\tilde{\bar{\boldsymbol{\delta}}}_r=\bar{\boldsymbol{\delta}}_r-\hat{\bar{\boldsymbol{\delta}}}_r$.

Deriving Eq. (20) with respect to time, we have

$$\dot{V}={z_{\mathrm{e}}}^{\mathrm{T}}\dot{z}_{\mathrm{e}}+\boldsymbol{\psi}_{\mathrm{e}}\dot{\boldsymbol{\psi}}_{\mathrm{e}}+\boldsymbol{u}_{\mathrm{e}}\dot{\boldsymbol{u}}_{\mathrm{e}}+\boldsymbol{r}_{\mathrm{e}}\dot{\boldsymbol{r}}_{\mathrm{e}}-\tilde{\bar{\boldsymbol{\delta}}}_u{\gamma_{d_u}}^{-1}\dot{\hat{\bar{\boldsymbol{\delta}}}}_u-\tilde{\bar{\boldsymbol{\delta}}}_r{\gamma_{d_r}}^{-1}\dot{\hat{\bar{\boldsymbol{\delta}}}}_r \tag{21}$$

where

$${z_{\mathrm{e}}}^{\mathrm{T}}\dot{z}_{\mathrm{e}}=-{z_{\mathrm{e}}}^{\mathrm{T}}k_{11}z_{\mathrm{e}}-\frac{{z_{\mathrm{e}}}^{\mathrm{T}}k_{12}z_{\mathrm{e}}}{\sqrt{\|z_{\mathrm{e}}\|^2+\varsigma^2}}+{z_{\mathrm{e}}}^{\mathrm{T}}\Delta_{\mathrm{e}}\leqslant -{z_{\mathrm{e}}}^{\mathrm{T}}k_{11}z_{\mathrm{e}}-\frac{{z_{\mathrm{e}}}^{\mathrm{T}}k_{12}z_{\mathrm{e}}}{\sqrt{\|z_{\mathrm{e}}\|^2+\varsigma^2}}+{z_{\mathrm{e}}}^{\mathrm{T}}\Delta_{\mathrm{e}}^{*} \tag{22}$$

$$\boldsymbol{\psi}_{\mathrm{e}}\dot{\boldsymbol{\psi}}_{\mathrm{e}}=-k_{31}{\boldsymbol{\psi}_{\mathrm{e}}}^2-\frac{k_{32}{\boldsymbol{\psi}_{\mathrm{e}}}^2}{\sqrt{\|\boldsymbol{\psi}_{\mathrm{e}}\|^2+\varsigma^2}}+\boldsymbol{\psi}_{\mathrm{e}}\boldsymbol{r}_{\mathrm{e}} \tag{23}$$

$$z_e^{\mathrm{T}}\dot{z}_e+\psi_e\dot{\psi}_e=-z_e^{\mathrm{T}}k_{11}z_e-\frac{z_e^{\mathrm{T}}k_{12}z_e}{\sqrt{\|z_e\|^2+\varsigma^2}}+$$
$$z_e^{\mathrm{T}}\Delta_e^*-k_{11}\psi_e^2-\frac{k_{32}\psi_e^2}{\sqrt{\|\psi_e\|^2+\varsigma^2}}+\psi_e r_e \tag{24}$$

According to the proof in Reference [21], we let $\kappa_{11}=\min\{k_{11},k_{31}\}$, $\Delta_e=ug_u(\psi)-u^*g_u(\psi^*)$, and there is Δ_e^* that meets $\|\Delta_e\|\leqslant\Delta_e^*$. Here, Δ_e^* is a constant.

We scale $u_e\dot{u}_e-\tilde{\bar{\delta}}_u\gamma_{d_u}^{-1}\dot{\hat{\delta}}_u$ and $r_e\dot{r}_e-\tilde{\bar{\delta}}_r\gamma_{d_r}^{-1}\dot{\hat{\delta}}_r$ as follows:

$$u_e\dot{u}_e-\tilde{\bar{\delta}}_u\gamma_{d_u}^{-1}\dot{\hat{\delta}}_u=u_e\left[-k_{21}u_e-\frac{k_{22}u_e}{\sqrt{\|u_e\|^2+\varsigma^2}}-\mathrm{Tanh}\left(\frac{u_e}{\varpi_u}\right)\hat{\bar{\delta}}_u+\right.$$
$$\left.\tilde{W}_u^{\mathrm{T}}\sigma(\eta)+\delta_u\right]-\tilde{\bar{\delta}}_u\left[\mathrm{Tanh}\left(\frac{u_e}{\varpi_u}\right)u_e-\lambda_{d_u}\hat{\bar{\delta}}_u\right]\leqslant$$
$$-k_{21}u_e^2-\frac{k_{22}u_e^2}{\sqrt{\|u_e\|^2+\varsigma^2}}-\frac{\lambda_{d_u}}{2}\tilde{\bar{\delta}}_u^2+$$
$$\frac{1}{4}\|\tilde{W}_u^{\mathrm{T}}\sigma(\eta)\|^2+u_e\left[\delta_u-\mathrm{Tanh}\left(\frac{u_e}{\varpi_u}\right)\bar{\delta}_u\right]+\frac{\lambda_{d_u}}{2}\bar{\delta}_u^2 \tag{25}$$

$$r_e\dot{r}_e-\tilde{\bar{\delta}}_r\gamma_{d_r}{}^{-1}\dot{\hat{\delta}}_r=r_e\left[-k_{41}r_e-\right.$$
$$\left.\frac{k_{42}r_e}{\sqrt{\|r_e\|^2+\varsigma^2}}-\psi_e-\mathrm{Tanh}\left(\frac{r_e}{\varpi_r}\right)\hat{\bar{\delta}}_r+\right.$$
$$\left.\tilde{W}_r^{\mathrm{T}}\sigma(\eta)+\delta_r\right]-\tilde{\bar{\delta}}_r\left[\mathrm{Tanh}\left(\frac{r_e}{\varpi_r}\right)r_e-\lambda_{d_r}\hat{\bar{\delta}}_r\right]\leqslant$$
$$-k_{41}r_e^2-\frac{k_{42}r_e^2}{\sqrt{\|r_e\|^2+\varsigma^2}}-$$
$$r_e\psi_e-\frac{\lambda_{d_r}}{2}\tilde{\bar{\delta}}_r^2+\frac{1}{4}\|\tilde{W}_r^{\mathrm{T}}\sigma(\eta)\|^2+$$
$$r_e\left[\delta_r-\mathrm{Tanh}\left(\frac{r_e}{\varpi_r}\right)\bar{\delta}_r\right]+\frac{\lambda_{d_r}}{2}\bar{\delta}_r^2 \tag{26}$$

where $\lambda_{d_u},\lambda_{d_r}$, ω_u, and ω_r are adjustable parameters in the design of the adaptive law.

According to Lemma 3, we have

$$\begin{cases}u_e\left[\delta_u-\mathrm{Tanh}\left(\dfrac{u_e}{\varpi_u}\right)\bar{\delta}_u\right]\leqslant 0.278\,5\varpi_u\bar{\delta}_u\\ r_e\left[\delta_r-\mathrm{Tanh}\left(\dfrac{r_e}{\varpi_r}\right)\bar{\delta}_r\right]\leqslant 0.278\,5\varpi_r\bar{\delta}_r\end{cases} \tag{27}$$

Since $\tilde{W}_u$, $\tilde{W}_r$ and $\sigma(\eta)$ are bounded, there is $\pi>0$, and $\|\tilde{W}_u^{\mathrm{T}}\|\leqslant\pi_u$, $\|\tilde{W}_u^{\mathrm{T}}\|\leqslant\pi_r$ are satisfied, According to Eqs. (25)-(27), we have

$$u_e\dot{u}_e-\tilde{\bar{\delta}}_u\gamma_{d_u}{}^{-1}\dot{\hat{\delta}}_u\leqslant-k_{21}u_e^2-\frac{k_{22}u_e^2}{\sqrt{\|u_e\|^2+\varsigma^2}}-$$
$$\frac{\lambda_{d_u}}{2}\tilde{\bar{\delta}}_u^2+\frac{\lambda_{d_u}}{2}\bar{\delta}_u^2+0.278\,5\varpi_u\bar{\delta}_u+\frac{1}{4}\pi_u^2 \tag{28}$$

$$r_e\dot{r}_e-\tilde{\bar{\delta}}_r\gamma_{d_r}{}^{-1}\dot{\hat{\delta}}_r\leqslant-k_{41}r_e^2-\frac{k_{42}r_e^2}{\sqrt{\|r_e\|^2+\varsigma^2}}-r_e\psi_e-$$
$$\frac{\lambda_{w_r}}{2}\tilde{\bar{\delta}}_r^2+0.278\,5\varpi_r\delta_r+\frac{1}{4}\pi_r^2 \tag{29}$$

By substituting Eqs. (24), (28), and (29) into Eq. (21), we have

$$\dot{V}\leqslant-z_e^{\mathrm{T}}\kappa_{11}z_e-\frac{z_e^{\mathrm{T}}k_{12}z_e}{\sqrt{\|z_e\|^2+\varsigma^2}}+z_e^{\mathrm{T}}\Delta_e^*-$$
$$\kappa_{11}\psi_e^2-\frac{k_{32}\psi_e^2}{\sqrt{\|\psi_e\|^2+\varsigma^2}}-k_{21}u_e^2-$$
$$\frac{k_{22}u_e^2}{\sqrt{\|u_e\|^2+\varsigma^2}}-\frac{\lambda_{d_u}}{2}\tilde{\bar{\delta}}_u^2+\frac{\lambda_{d_u}}{2}\bar{\delta}_u^2+0.278\,5\varpi_u\bar{\delta}_u-$$
$$k_{41}r_e^2-\frac{k_{42}r_e^2}{\sqrt{\|r_e\|^2+\varsigma^2}}-\frac{\lambda_{d_r}}{2}\tilde{\bar{\delta}}_r^2+\frac{\lambda_{d_r}}{2}\bar{\delta}_r^2+$$
$$0.278\,5\varpi_r\bar{\delta}_r+\Lambda\leqslant-z_e^{\mathrm{T}}\kappa_{11}z_e-\kappa_{12}\|z_e\|-\kappa_{11}\psi_e^2-$$
$$\kappa_{12}\|\psi_e\|-\kappa_{21}u_e^2-\kappa_{22}\|u_e\|-\frac{\lambda_{d_u}}{2}\tilde{\bar{\delta}}_u^2+\frac{\lambda_{d_u}}{2}\bar{\delta}_u^2+$$
$$0.278\,5\varpi_u\bar{\delta}_u+\varsigma[\kappa_{12}+\kappa_{22}]+\Lambda \tag{30}$$

where $\Lambda=\Delta_e^*+\frac{1}{4}\pi_u^2+\frac{1}{4}\pi_r^2$, $\kappa_{11}=\min\{k_{11},k_{31}\}$, $\kappa_{12}=\min\{k_{12},k_{32}\}$, $\kappa_{21}=\min\{k_{21},k_{41}\}$, and $\kappa_{22}=\min\{k_{22},k_{42}\}$.

According to Young's inequality, we have

$$\begin{cases}\dfrac{\lambda_{d_u}}{4}\|\tilde{\bar{\delta}}_u\|\leqslant\dfrac{\lambda_{d_u}}{4}\|\tilde{\bar{\delta}}_u\|^2+\dfrac{\lambda_{d_u}}{16}\\ \dfrac{\lambda_{d_r}}{4}\|\tilde{\bar{\delta}}_r\|\leqslant\dfrac{\lambda_{d_r}}{4}\|\tilde{\bar{\delta}}_r\|^2+\dfrac{\lambda_{d_r}}{16}\end{cases} \tag{31}$$

Substituting Eq. (31) into Eq. (30), we can further obtain

$$\dot{V}\leqslant-z_e^{\mathrm{T}}\kappa_{11}z_e-\kappa_{12}\|z_e\|-\kappa_{21}u_e^2-\kappa_{11}\psi_e^2-\kappa_{12}\|\psi_e\|-$$
$$\kappa_{21}r_e^2-\kappa_{22}\|u_e\|-\frac{\lambda_{d_u}}{4}\tilde{\bar{\delta}}_u^2-\frac{\lambda_{d_u}}{4}\|\tilde{\bar{\delta}}_u\|+\frac{\lambda_{d_u}}{2}\bar{\delta}_u^2+$$
$$0.278\,5\varpi_u\bar{\delta}_u-\kappa_{22}\|r_e\|-\frac{\lambda_{d_r}}{4}\tilde{\bar{\delta}}_r^2-\frac{\lambda_{d_r}}{4}\|\tilde{\bar{\delta}}_r\|+\frac{\lambda_{d_r}}{2}\bar{\delta}_r^2+$$
$$0.278\,5\varpi_r\bar{\delta}_r+\frac{1}{16}(\lambda_{d_u}+\lambda_{d_r})+\varsigma[\kappa_{12}+\kappa_{22}]+\Lambda\leqslant$$
$$-\frac{\rho_1}{2}\left(z_e^{\mathrm{T}}z_e+u_e^2+\tilde{\bar{\delta}}_u^{\mathrm{T}}\lambda_u^{-1}\tilde{\bar{\delta}}_u+\psi_e^2+r_e^2+\tilde{\bar{\delta}}_r^{\mathrm{T}}\lambda_r^{-1}\tilde{\bar{\delta}}_r\right)-$$
$$\rho_2\left[\left(\frac{1}{2}z_e^{\mathrm{T}}z_e\right)^{\frac{1}{2}}+\left(\frac{1}{2}u_e^2\right)^{\frac{1}{2}}+\left(\frac{1}{2\lambda_u}\tilde{\bar{\delta}}_u^{\mathrm{T}}\tilde{\bar{\delta}}_u\right)+\left(\frac{1}{2}\psi_e^2\right)^{\frac{1}{2}}+\right.$$
$$\left.\left(\frac{1}{2}r_e^2\right)^{\frac{1}{2}}+\left(\frac{1}{2\lambda_r}\tilde{\bar{\delta}}_r^{\mathrm{T}}\tilde{\bar{\delta}}_r\right)\right]+\theta\leqslant-\rho_1V-\rho_2V^{\frac{1}{2}}+\theta \tag{32}$$

$$\rho_1=\min\left\{2\kappa_{11},2\kappa_{21},\frac{\kappa_\lambda}{2}\kappa_\gamma\right\} \tag{33}$$

$$\rho_2=2^{\frac{1}{2}}\min\left\{\kappa_{12},\kappa_{22},\frac{\kappa_\lambda}{4}\lambda_m^{1/2}(\kappa_\gamma)\right\} \tag{34}$$

$$\kappa_\lambda=\min\{\lambda_{d_u},\lambda_{d_r}\},\ \kappa_\gamma=\min\{\gamma_{d_u},\gamma_{d_r}\} \tag{35}$$

$$\theta=\frac{\kappa_\lambda}{2}\left(\bar{\delta}_u^2+\bar{\delta}_r^2\right)+0.278\,5\left(\varpi_u\bar{\delta}_u+\varpi_r\bar{\delta}_r\right)+$$
$$\frac{\kappa_\lambda}{16}+\varsigma[k_{12}+k_{22}]+\Lambda \tag{36}$$

From Eq. (32), we have

$$\dot{V}\leqslant-\eta\rho_1V-(1-\eta)\rho_1V-\rho_2V^{\frac{1}{2}}+\theta \tag{37}$$

where $\eta = \min\{\eta_1, \eta_2\}$, $0 < \eta < 1$.

According to Eq. (29), we have $V > \dfrac{\theta}{\eta\rho_1}$ and then

$$\dot{V} \leqslant -(1-\eta)\rho_1 V - \rho_2 V^{\frac{1}{2}} \tag{38}$$

According to Lemma 1, it is known that the system will be stable in the area $\Omega_v = \left\{V : V \leqslant \dfrac{\theta}{\eta\rho_1}\right\}$ within a finite time, and the stabilization time is

$$T \leqslant \frac{4}{(1-t)\rho_1}\ln\left[\frac{(1-t)\rho_1 V^{\frac{1}{2}}(0)+\rho_2}{\rho_2}\right] \tag{39}$$

where $V(0)$ is the initial value of V.

According to Eq. (22), the above calculation proves that for $\forall t \geqslant T$, the system error will converge within a finite time.

4 Simulation research

In order to verify the effectiveness of the control scheme design in this paper, we use the Cybership 2 ship model of Norwegian University of Science and Technology as the controlled object for the computer simulation test. This model has a total length L of 1.255 m and a mass m of 23.8 kg, with other hydrodynamic parameters presented in Reference [22].

In the simulation analysis, we compare the control scheme in this paper with the control scheme based on the adaptive neural network without finite time. In the simulation diagram, we set the control law designed in this paper as Control law 1 and the control law used for comparison as Control law 2. The virtual control law, control law, and adaptive law of the control law used for comparison are shown in Eqs. (40)-(43).

$$\begin{cases}\alpha = -k_{11}z_e - v\boldsymbol{g}_v(\psi) + \begin{pmatrix}\dot{x}_1\\ \dot{y}_1\end{pmatrix}\\ \alpha_r = -k_{31}\psi_e + \dot{\psi}_1\end{cases} \tag{40}$$

$$\begin{cases}\tau_u = m_u\left[-k_{21}u_e - \hat{W}_u^{\mathrm{T}}\sigma(\eta) + \dot{u}_1 - \mathrm{Tanh}\left(\dfrac{u_e}{\varpi_u}\right)\hat{\bar{\delta}}_u\right]\\ \tau_r = m_r\left[-k_{41}r_e - \hat{W}_r^{\mathrm{T}}\sigma(\eta) + \dot{r}_1 - \psi_e - \mathrm{Tanh}\left(\dfrac{r_e}{\varpi_r}\right)\hat{\bar{\delta}}_r\right]\end{cases} \tag{41}$$

$$\begin{cases}\dot{\hat{W}}_u = \gamma_{w_u}[u_e\sigma(\eta) - \lambda_{w_u}\|u_e\|\hat{W}_u]\\ \dot{\hat{W}}_r = \gamma_{w_r}[r_e\sigma(\eta) - \lambda_{w_r}\|r_e\|\hat{W}_r]\end{cases} \tag{42}$$

$$\begin{cases}\dot{\hat{\bar{\delta}}}_u = \gamma_{d_u}\left(\mathrm{Tanh}\left(\dfrac{u_e}{\varpi_u}\right)u_e - \lambda_{d_u}\hat{\bar{\delta}}_u\right)\\ \dot{\hat{\bar{\delta}}}_r = \gamma_{d_r}\left(\mathrm{Tanh}\left(\dfrac{r_e}{\varpi_r}\right)r_e - \lambda_{d_r}\hat{\bar{\delta}}_u\right)\end{cases} \tag{43}$$

In order to simulate the sea state, the disturbances are calculated by Eq. (44):

$$\begin{cases}d_u = 0.1 + 0.01(\sin(-1.1t) + 1.5\sin(-0.8t))\\ d_v = 0.01(1.2\sin(0.1t) + 1.5\sin(-0.1t))\\ d_r = 0.1 + 0.02(-\sin(2t) - 4\sin(t))\end{cases} \tag{44}$$

When the model parameters are unknown, we set the parameters $k_{11} = 0.1$, $k_{12} = 0.1$, $k_{21} = 0.2$, $k_{22} = 0.1$, $k_{31} = 0.2$, $k_{32} = 0.05$, $k_{41} = 0.4$, $k_{42} = 0.05$, $\gamma_{d_u} = 0.1$, $\gamma_{d_r} = 1$, $\lambda_{d_r} = 1$, $\gamma_{w_u} = \gamma_{w_r} = 200$ and $\lambda_{w_u} = \lambda_{w_r} = 0.002\,5$. The simulation test adopts the circular trajectory equation, as shown in Eq. (45):

$$\begin{cases}x_1 = 25\sin(0.01t)\\ y_1 = 25 - 25\cos(0.01\pi t)\end{cases} \tag{45}$$

Under the circular trajectory, the initial position and speed of the ship are expressed as follows: (x_0; y_0; ψ_0; u_0; v_0; r_0) = (0; 10; 0; 0; 0; 0).

Figs. 2-9 show the simulation results under the circular trajectory. Specifically, Fig. 2 compares the actual trajectories of Control law 1 and Control law 2 and their reference trajectories, and it is indicated that the actual trajectories in the proposed control scheme are closer to the reference trajectories within a finite time.

Figs. 3-6 compare the position tracking, course angle tracking, and speed tracking of ships under different control laws. It can be seen that the controller designed in this paper can ensure that it is closer to the desired trajectory within a finite time.

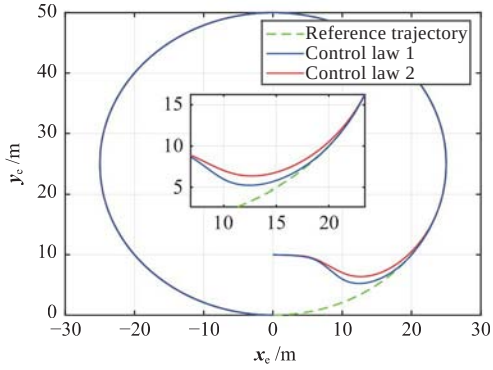

Fig. 2 Actual and reference trajectories of ship in (x, y) plane

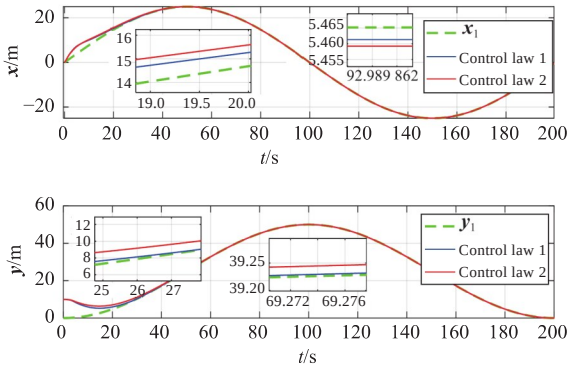

Fig. 3 Actual and reference positions

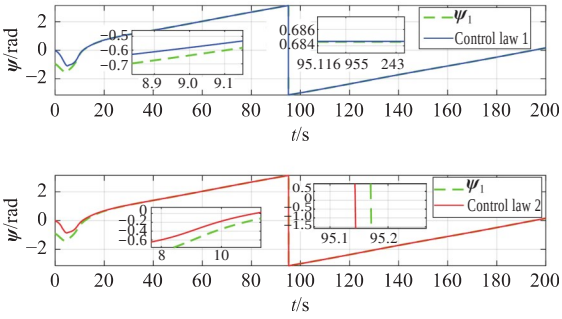

Fig. 4 Actual and expected course angles

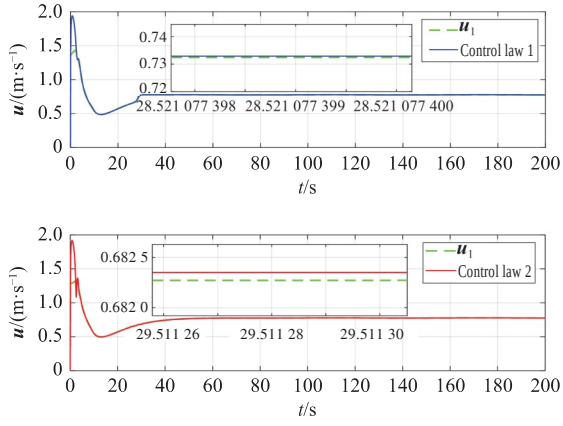

Fig. 5 Surge velocity $\boldsymbol{u}$

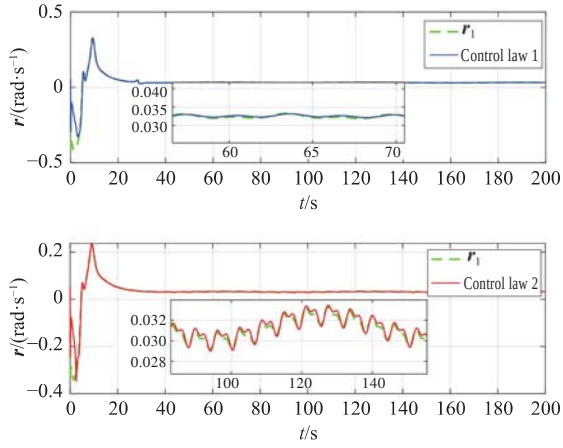

Fig. 6 Heading rate $\boldsymbol{r}$

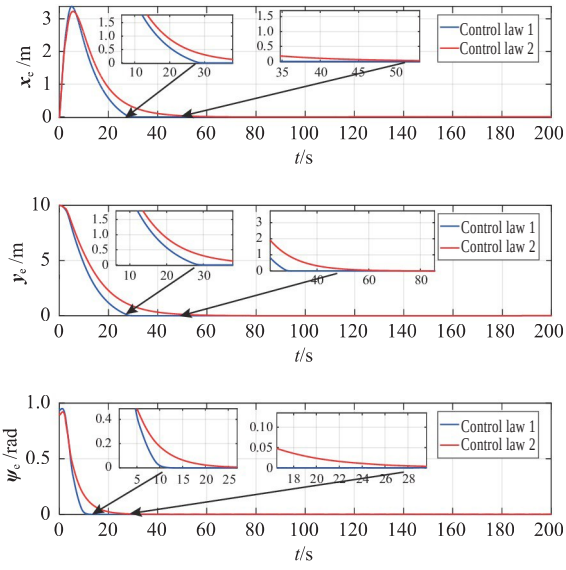

Fig. 7 Time history curves of pose error

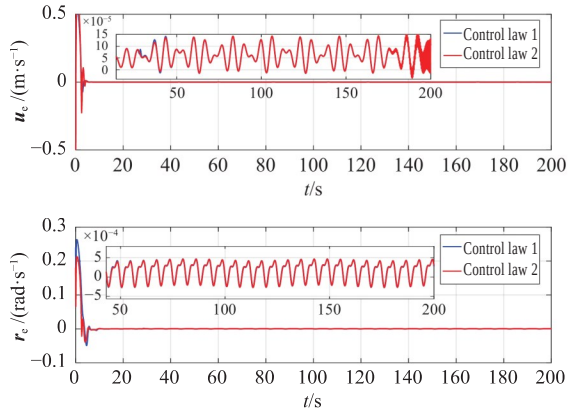

Fig. 8 Time history curves of speed error

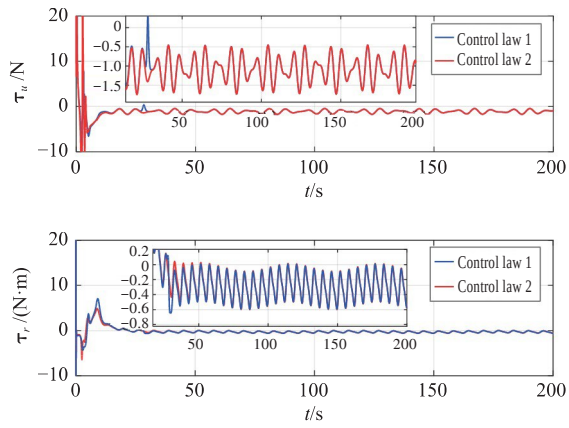

Fig. 9 Control input of $\boldsymbol{\tau}_u$ and $\boldsymbol{\tau}_r$

Fig. 7 shows the time history curves of pose error. It is indicated that the upper and lower bounds of the error in the designed control scheme are smaller, and under the finite-time control scheme, $\boldsymbol{x}_e$ and $\boldsymbol{y}_e$ converge at about 29 s, and $\boldsymbol{\psi}_e$ converges at about the 10 s, while the pose error of the comparison scheme converges at about 50, 55, and 28 s, respectively. This suggests that the designed control scheme in this paper has a faster convergence speed.

According to the time history curves of speed error in Fig. 8, the convergence of the speed error of the control scheme designed in this paper has improved to some extent, and its upper and lower bounds are also smaller.

Fig. 9 presents the curves of control input with time. It can be seen that the input of the control law designed in this paper displays no obvious increase compared with the one used for comparison.

5 Conclusion

The finite-time trajectory tracking control scheme based on an adaptive neural network proposed in this paper has solved the problems of unknown disturbances and dynamic uncertainties in the trajectory tracking of underactuated ships, and the control accuracy of the system and the conver-

gence speed of the system error have been improved. Using the RBF neural network, we reconstruct unknown dynamics and design an adaptive law to approximate the upper bound of external disturbances. Through the Lyapunov theory, it is proved that all signals of the underactuated ship system are bounded. The simulation comparison with the adaptive neural network control law without finite time is carried out, and the result shows that the control scheme designed in this paper has better tracking performance. In subsequent work, we will study how to simplify the complexity of the algorithm while improving tracking accuracy.

References

[1] GE H, JING Z L, GAO J. Trajectory tracking of fully actuated AUV based on TLC method [J]. Journal of Shanghai Jiaotong University, 2011, 45(2): 184−189. (in Chinese)

[2] SHEN Z P, ZHANG X L. Recursive sliding-mode dynamic surface adaptive control for ship trajectory tracking with nonlinear gains [J]. Acta Automatica Sinica, 2018, 44(10): 1833−1841. (in Chinese)

[3] SHEN Z P, BI Y N, WANG Y, et al. Adaptive recursive sliding mode control for surface vessel trajectory tracking with input and output constraints [J]. Control Theory & Application, 2020, 37(6): 1419−1427. (in Chinese)

[4] MENG W, GUO C, SUN F C, et al. Nonlinear sliding mode tracking control of underatuated surface vessels [J]. Journal of Harbin Engineering University, 2012, 33 (5): 585−589. (in Chinese)

[5] SHEN Z P, BI Y N, GUO T T, et al. Adaptive dynamic surface output feedback trajectory tracking control for underactuated ships with nonlinear observer [J]. Systems Engineering and Electronics, 2019, 41(2): 409−415. (in Chinese)

[6] LIU C G, CHU X M, WANG L, et al. Trajectory tracking controller for underactuated surface vessels based on model predictive control [J]. Journal of Shanghai Jiaotong University, 2015, 49(12):1842−1848, 1854. (in Chinese)

[7] DU J L, HU X, KRSTIĆM, et al. Dynamic positioning of ships with unknown parameters and disturbances [J]. Control Engineering Practice, 2018, 76: 22−30.

[8] SUN Z J, ZHANG G Q, QIAO L, et al. Robust adaptive trajectory tracking control of underactuated surface vessel in fields of marine practice [J]. Journal of Marine Science and Technology, 2018, 23(6): 950−957.

[9] DAI S L, HE S, WANG M, et al. Adaptive neural control of underactuated surface vessels with prescribed performance guarantees [J]. IEEE Transactions on Neural Networks and Learning Systems, 2019, 30(12): 3686−3698.

[10] HASELTABLE A, NEGENBORN R R. Adaptive control for autonomous ships with uncertain model and unknown propeller dynamics [J]. Control Engineering Practice, 2019, 91: 104116.

[11] WANG Y Q, LI T S. Finite-time trajectory tracking control of under-actuated surface vessel [J]. Journal of Harbin Engineering University, 2017, 38(5): 684−689. (in Chinese)

[12] NING W, MENG J E. Direct adaptive fuzzy tracking control of marine vehicles with fully unknown parametric dynamics and uncertainties [J]. IEEE Transactions on Control Systems Technology, 2016, 24(5): 1845−1852.

[13] SUN K K, QIU J B, KARIMI H R, et al. Event-triggered robust fuzzy adaptive finite-time control of nonlinear systems with prescribed performance [J]. IEEE Transactions on Fuzzy Systems, 2021, 29 (6): 1460−1471.

[14] ZHAO L, YU J P, YU H S. Adaptive finite-time attitude tracking control for spacecraft with disturbances [J]. IEEE Transactions on Aerospace and Electronic Systems, 2018, 54(3): 1297−1305.

[15] DENG Y P, ZHANG X K, IM N, et al. Model-based event-triggered tracking control of underactuated surface vessels with minimum learning parameters [J]. IEEE Transactions on Neural Networks and Learning Systems, 2020, 31(10): 4001−4014.

[16] WANG F, CHEN B, LIU X P, et al. Finite-time adaptive fuzzy tracking control design for nonlinear systems [J]. IEEE Transactions on Fuzzy Systems, 2018, 26(3): 1207−1216.

[17] HUANG Y, JIA Y M. Adaptive fixed-time six-DOF tracking control for noncooperative spacecraft fly-around mission [J]. IEEE Transactions on Control Systems Technology, 2019, 27(4): 1796−1804.

[18] ZHANG Q, ZHU G B, HU X, et al. Adaptive neural network auto-berthing control of marine ships [J]. Ocean Engineering, 2019, 177: 40−48.

[19] XU B, SHOU Y X. Composite learning control of MIMO systems with applications [J]. IEEE Transactions on Industrial Electronics, 2018, 65(8): 6414−6424.

[20] POLYCARPOU M M. Stable adaptive neural control scheme for nonlinear systems [J]. IEEE Transactions on Automatic Control, 1996, 41(3): 447−451.

[21] WU W T, GU N, PENG Z H, et al. Distributed time-varying formation control for unmanned surface vehicles guided by multiple leaders [J]. Chinese Journal of Ship Research, 2020, 15(1): 21−30. (in Chinese)

[22] SKJETNE R, FOSSEN T I, KOKOTOVI P V. Adaptive maneuvering, with experiments, for a model ship in a marine control laboratory [J]. Automatica, 2005, 41(2): 289−298.

欠驱动船舶自适应神经网络有限时间轨迹跟踪

张强, 朱雅萍, 孟祥飞, 张树豪*, 胡宴才
山东交通学院 航运学院, 山东 威海 264200

摘　要: [**目的**] 针对欠驱动水面船舶在轨迹跟踪控制中存在的动态不确定和未知扰动问题, 设计一种自适应神经网络有限时间轨迹跟踪控制方案。[**方法**] 利用运动学虚拟控制律变换和有界限制的方法进行欠驱动变化。在 Backstepping 的框架下, 利用神经网络重构未知动态, 并设计自适应律逼近未知扰动的上界。通过 Lyapunov 直接法提供严格的理论分析, 以证明闭环系统所有信号都是有界的, 并使跟踪误差收敛至有界的区间。[**结果**] 仿真结果表明, 所提控制方案能够使欠驱动船舶在有限的时间内跟踪上期望的轨迹, 且相比传统控制方案, 系统误差的收敛速度更快, 误差的上、下界也更小, 在面对外界未知的时变干扰时还具有良好的鲁棒性。[**结论**] 所做研究可为船舶的轨迹跟踪控制提供有效参考, 具有实际的工程意义。

关键词: 轨迹跟踪; 自适应神经网络; 有限时间; 不确定扰动; 欠驱动水面船舶